

Article

Energy Gap-Refractive Index Relations in Perovskites

Aneer Lamichhane ^{1,2,†}  and Nuggehalli M. Ravindra ^{1,2,*,†} 

¹ Interdisciplinary Program in Materials Science & Engineering, New Jersey Institute of Technology, Newark, NJ 07102, USA; al593@njit.edu

² Department of Physics, New Jersey Institute of Technology, Newark, NJ 07102, USA

* Correspondence: nmravindra@gmail.com

† These authors contributed equally to this work.

Received: 20 February 2020; Accepted: 15 April 2020; Published: 19 April 2020



Abstract: In this study, the energy gap-refractive index relations of perovskites are examined in detail. In general, the properties of perovskites are dependent on the structural reorganization and covalent nature of their octahedral cages. Based on this notion, a simple relation governing the energy gap and the refractive index is proposed for perovskites. The results obtained with this relation are in good accord with the literature values and are consistent with some well-established relations.

Keywords: energy gap; refractive index; perovskites

1. Introduction

Perovskites are materials having the crystal structure of strontium titanate at room temperature ($SrTiO_3$) with a general formula for the oxide analogs of ABX_3 , where A is a cation, generally a rare-earth- or alkali-type element, B is a transition metal cation, and X is an oxide or halide anion [1–3]. In recent years, there has been a growing interest among material scientists in the study of perovskites [4–6]. This is because perovskites exhibit a variety of functions such as piezoelectric, pyroelectric, ferroelectric, photovoltaic cells, LEDs, superconductivity, and topological insulators [7–10]. Generally, oxide perovskites exhibit good dielectric properties, and halide perovskites show excellent photonic properties [11,12]. Since the discovery of calcium titanium oxide, $CaTiO_3$, by Gustav Rose in 1839, the research on perovskites remained dormant until the 21st Century [13,14]. The first paper on lead halide perovskites was published in 1892 [15]. The structure of $CsPbI_3$, cesium plumbo iodide, was studied in 1959 [16]. It is only in the last decade that perovskites have gained notoriety as materials for photovoltaic conversion. The paper “Organometal Halide Perovskites as Visible-Light Sensitizers for Photovoltaic Cells” by Kojima and Miyasaka et al. [17] has been the catalyst for the exponential growth of research on perovskite solar cells. Due to their inherent direct energy gap that matches the solar spectrum, halide perovskites continue to perform well as photonic materials [18,19]. Moreover, the crystal structures of perovskites show different polymorphs [20–22], which further contribute to significant changes in their dielectric and photonic properties.

It is, therefore, crucial to understand the electronic and optical properties of perovskites to predict the behavior of these functionalities. Such predictions are useful to engineer these materials for various applications. Among several properties, the energy gap and the refractive index are fundamental entities whose correlation is vital for the understanding of the optoelectronic behavior of materials, as well as band-gap engineering [23–26]. While the threshold wavelength for the absorption of photons in semiconductors is determined by the energy gap, the transparency to incident spectral radiation is quantified by the refractive index. Such a correlation between these two fundamental properties is critical for the determination of the choice of semiconductors for applications in electronics and photonics [27]. Several studies about the relationship between the energy gap and the refractive index

have been proposed for semiconductors and examined in the past, yielding various theories in this field [27–29]. There has been renewed interest in these studies in recent years [30–37]. While several manuscripts have reported on the studies of the energy gap and refractive index of perovskites [38–41], Blessing N. Ezealigo et.al. [42] performed a detailed experimental investigation into their research entitled “Method to control the optical properties: Band gap energy of mixed halide Organolead perovskites”, and the results obtained have been interpreted by utilizing the single-oscillator model of Wemple–DiDomenico.

To the best of our knowledge and understanding, a detailed study of the correlations between the refractive index and energy gap for all inorganic perovskites is lacking in the literature. This is the first study of its kind being reported here. A comprehensive study of the fundamental properties such as the energy gap and refractive index is of paramount importance for the study of materials, in particular perovskites, since they are the basis for determining their applications in electronics and photonics. Furthermore, computational frameworks in materials science such as “propnet” [34] require pre-knowledge of the database of these material properties. As materials informatics begins to grow, investigations such as these that relate two fundamental macroscopic properties will pave the way for new applications of perovskites.

2. Background

From a fundamental point of view, the refractive index of a material is simply defined as the ratio of the speed of light in a vacuum to that in the material. In general, the refractive index of a material is a function of (a) frequency and (b) doping, although studies in the literature report on the dependence of the refractive index on thickness [43], voids [44], grain boundaries [45], etc. In order to minimize such variation, it is good practice to consider a static refractive index, which is obtained from the time-independent electric field or the field at a zero wave vector. In 1950, Moss [46,47] proposed the general relationship between the energy gap (E_g) and the refractive index (n) as,

$$n^4 E_g = 95 eV \quad (1)$$

This model is based on Bohr’s atomic model of hydrogen. The assumption was that all energy levels in a solid are scaled down by a factor of $\frac{1}{\epsilon_\infty}$, where ϵ_∞ is the optical dielectric constant satisfying the relation [48],

$$\epsilon_\infty = n^2 \quad (2)$$

Since energy levels in a solid are quite complex and involve band structure theory, this gives rise to a structural restriction on Moss’s relation. Based on the band structure, in 1962, Penn [49] proposed a model for an isotropic semiconductor by modifying Callaway’s approximation of the dielectric constant with the inclusion of the Umklapp process and showed the relation,

$$\epsilon_\infty = 1 + (\hbar\omega_p/E_g)^2, \quad (3)$$

where ω_p is the plasma frequency [50]. Almost, in all semiconductors, the trajectories of valence and conduction bands are more or less parallel with each other, at least along the symmetry directions. With these considerations, Gupta and Ravindra [51] proposed that the difference between the Penn gap and the energy gap is constant and showed the linear relationships between the energy gap and the refractive index as [52],

$$n = 4.084 - 0.62E_g(eV) \quad (4)$$

However, Equation (4) puts an upper limit on the refractive index. In order to account for both the structural and the refractive index restriction of the Moss relation and the Ravindra relation,

respectively, several empirical relations have been presented by various authors [29,53,54]. Based on the oscillatory theory, Herve and Vandamme [55] presented the relation,

$$n = \sqrt{1 + \left(\frac{A}{E_g + B}\right)^2} \quad (5)$$

where $A = 13.6$ eV and $B = 3.4$ eV are the constants. Though this relation is quite superior and agrees satisfactorily for most optoelectronic materials, it has shortcomings for materials of the IV-VI group [56].

In light of these drawbacks, this paper examines the correlations between the energy gap and the refractive index in perovskites. Utilizing the Wemple–DiDomenico single electron oscillator approximation [57] and based on the structure of perovskites, a simple relation is proposed for such ternary systems. Later, this model is compared with the Moss (Equation (1)), Ravindra (Equation (4)), and Herve–Vandamme (Equation (5)) models, as well as the reported experimental values of the refractive indices of perovskites in the literature.

3. Theory

The dependence of the refractive index (n) on the wavelength (λ) or frequency (ν) has been well described by dispersion relations. The first dispersion relation was developed by Cauchy [58],

$$n(\lambda) = A + \frac{B}{\lambda^2} + \frac{C}{\lambda^4} \quad (6)$$

where A , B , and C are constants. The Cauchy dispersion relation is simply an empirical fitting and bears no physical significance. A more significant dispersion model was given by Sellmeier [59],

$$n^2(\lambda) = 1 + \sum_i \frac{A_i \lambda^2}{\lambda^2 - \lambda_i^2} \quad (7)$$

where A_i is a constant and subscript i denotes the multiple resonant wavelengths. The Sellmeier dispersion relation represents a more realistic model as whenever the electric field is impinged on a material, the electron clouds get disturbed by it, and the nuclei exert a restoring force, yielding the possibilities of multiple excitation. Since both of these Cauchy and Sellmeier relations are empirical, the concrete formulation for the dispersion relation was given by the Drude–Lorentz electronic theory [60]. This theory assumes that the electric field applied on an electron bound to the nucleus exerts Hooke's force. Based on this model, it was found that the refractive index is associated with the oscillator strength (C_i) by [61],

$$n^2(\omega) = 1 + \frac{Ne^2}{2\pi m} \sum_i \frac{C_i}{\omega_i^2 - \omega^2} \quad (8)$$

where N is the particle density, e and m are the charge and mass of the electron, and ω_i and ω are the absorption and incident frequency, respectively. For a single oscillator, Wemple and DiDomenico introduced the semi-empirical relationship of the form [62,63],

$$n^2(\nu) - 1 = \frac{E_d E_o}{E_o^2 - (h\nu)^2} \quad (9)$$

where ν is the frequency, h is the Planck constant, E_o is the single oscillator energy, and E_d is the dispersion energy. The dispersion energy measures the average strength of interband optical transitions and is given by [62,63],

$$E_d = \beta N_c N_e Z_a (eV), \quad (10)$$

where N_c is the coordination number of the cation, N_e is the effective number of valence electrons per anion, Z_a is the formal charge of the anion, and β is a constant having the value 0.26 ± 0.04 eV for ionic compounds and 0.37 ± 0.05 eV for covalent compounds. Furthermore, based on the experimental data tested on several materials, it has been estimated empirically that the oscillator energy is related to the lowest energy gap by [62,63],

$$E_o \approx 1.5E_g \quad (11)$$

where E_g is the lowest direct band gap. Using the values of N_c , N_e , Z_a , and β for the perovskite structure in Equations (9)–(11), the Wemple and DiDomenico form for the static refractive index ($n(0)$ or simply n) can be written as,

$$n = \sqrt{1 + \frac{16.64eV}{E_g}} \quad (12a)$$

$$n = \sqrt{1 + \frac{8.32eV}{E_g}} \quad (12b)$$

for oxide perovskites and halide perovskites, respectively.

These Equation (12a) and (12b) are based on the fact that the optoelectronic properties of perovskites are dependent on the ionic nature of the bonds or by simply treating perovskites as ionic solids. It is unambiguously known today that the octahedral cage in perovskites is formed by the heteropolar bonds (mixed ionic/covalent interactions) among the B cation and X anions, whereas the cation A shows electrostatic interaction with this cage [64,65]. A majority of the school of thought claims that the properties of perovskites are dependent on the octahedral cage built from the interaction of $B - X$ ions, and the role of cation A is merely for the charge neutrality of the final stable structure [66–68]. In other words, the properties of perovskites evolve from the octahedral frame of $B - X$ ions, and the cation A affects those properties by distorting this frame. Moreover, this claim can be justified by the Pauling rule [69], as in a multication system, cations with high valency and a small coordination number (CN) form polyhedra with the anion and the cation with low valency and a high coordination number (CN) adjusting their positions for final stability. The cation/anion ratio, as suggested by Pauling, determines the coordination number (CN), which in turn determines the structure of the polyhedra. In the case of perovskites, we take the cation/anion ratio as the average ratio for two cations, i.e., $\frac{(r_A + r_B)}{2r_X}$, where r_A , r_B , and r_X are the ionic radii of A , B , and X at CNs 12, 6, and 2, respectively [70].

Henceforth, one can paraphrase that the properties of perovskites are dependent on the octahedral cage created by $B - X$ ions, and the adjustments of cation A for the final stable structure may lead to distorting this octahedral frame, which in turn influences these properties. Furthermore, the distortion of the octahedral cage induced by cation A may depend on the covalent nature of the $B - X$ bond [71,72]. The greater the covalent $B - X$ bond, the less is the distortion of the structure of ABX_3 . Finally, incorporating the covalent nature of the $B - X$ bond with the adjustment of A for the final stable structure, we propose the following modification of the Wemple and DiDomenico form,

$$n = \sqrt{1 + \frac{(r_A + r_B)}{r_X} \frac{11.84eV}{E_g}} \quad (13a)$$

$$n = \sqrt{1 + \frac{(r_A + r_B)}{r_X} \frac{5.92eV}{E_g}} \quad (13b)$$

for oxide perovskites and halide perovskites, respectively.

4. Results and Discussion

I. Validity of the model: Based on Equation (13a) and (13b), we calculated the refractive index values of various oxide perovskites and halide perovskites. The results were then compared with the literature values obtained from various sources as shown in Table 1, and the resulting data are further plotted in Figure 1. One can notice that the computed results using (13a) and (13b) were in agreement with the corresponding literature values. These could further be compared with the values obtained from the Wemple–DiDomenico relation, Moss relation, Ravindra relation, and Herve–Vandamme relation. It must be noted that the reference values of the refractive index were not homogeneous in terms of the wavelength used, whereas the refractive index calculated by Equation (13a) and (13b) corresponded to the static or low-frequency values. Thus, this factor may contribute to some error during the comparison. Furthermore, we calculated the absolute accuracy error ($AAE = |X_{standard} - X_{calculated}|$) and mean absolute error ($MAE = average(AAE)$) to reckon the deviation of the proposed relation along with the other established relations with their corresponding refractive indices. It can be seen that the proposed model showed a mean absolute error of 0.07, which was the smallest of all the other established models.

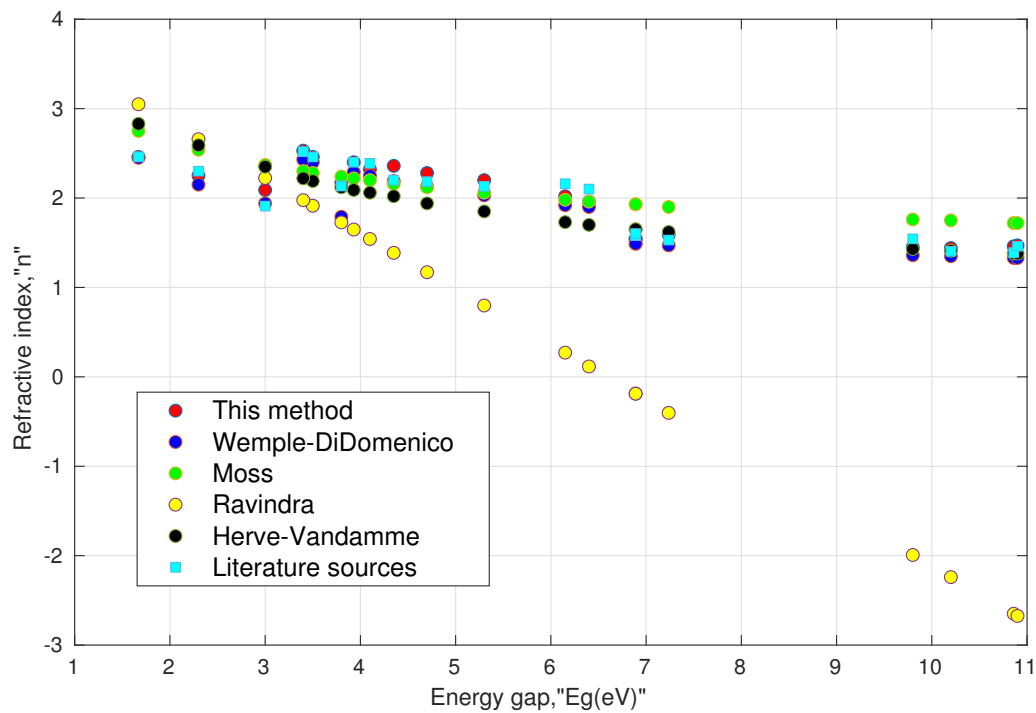


Figure 1. Comparison of various models with available literature data for perovskites, shown in Table 1.

Table 1. Comparison of refractive indices computed by various models with the literature values. AAE, absolute accuracy error.

Perovskite ABX_3	Energy Gap ' E_g (eV)'	Refractive Index ' n '	This Method (Equation (13a) and (13b))	AAE	Wemple- DiDomenico Relation (Equation (12a) and (12b))	AAE	Moss Relation (Equation (1))	AAE	Ravindra Relation (Equation (4))	AAE	Herve- Vandamme Relation (Equation (5))	AAE
$SrTiO_3$	4.1 [73]	2.388 (632.8 nm) [73]	2.32	0.07	2.25	0.14	2.20	0.19	1.54	0.85	2.06	0.33
$SrSnO_3$	3.93 [74]	≈ 2.4 [75]	2.40	0.00	2.29	0.11	2.22	0.18	1.65	0.75	2.09	0.31
$KMgF_3$	10.2 [76]	1.404 (632.8 nm) [73]	1.44	0.04	1.35	0.05	1.75	0.35	N.V.	N.D.	1.41	0.01
$CaTiO_3$	3.5 [77]	≈ 2.46 [78]	2.46	0.00	2.40	0.06	2.28	0.18	1.91	0.55	2.19	0.27
$PbTiO_3$	3.4 [79]	2.52 [80]	2.53	0.01	2.43	0.09	2.30	0.22	1.98	0.54	2.22	0.3
$CsPbF_3$	3.8 [81]	2.134 (5.7 eV) [81]	2.17	0.04	1.79	0.34	2.24	0.11	1.73	0.40	2.12	0.01
$CsPbI_3$	1.67 [82]	2.46 (435 nm) [82]	2.46	0.00	2.45	0.01	2.75	0.29	3.05	0.59	2.83	0.37
$KTaO_3$	4.35 [83]	2.2 (632.8 nm) [73]	2.36	0.16	2.19	0.01	2.16	0.04	1.39	0.81	2.02	0.18
$CsPbBr_3$	2.3 [84]	≈ 2.3 (580 nm) [85]	2.25	0.05	2.15	0.15	2.54	0.24	2.66	0.36	2.59	0.29
$CsPbCl_3$	3.0 [84]	≈ 1.91 [86]	2.09	0.18	1.94	0.03	2.37	0.46	2.22	0.31	2.35	0.44
$LiTaO_3$	4.7 [87]	≈ 2.183 (632.8 nm) [73]	2.28	0.10	2.13	0.05	2.12	0.06	1.17	1.01	1.94	0.24
$BaZrO_3$	5.30 [88]	2.13 [89]	2.20	0.07	2.03	0.10	2.06	0.07	0.80	1.33	1.85	0.28
$SrZrO_3$	6.15 [88]	2.16 [90]	2.02	0.14	1.92	0.24	1.98	0.18	0.27	1.89	1.73	0.43
$CaZrO_3$	6.40 [88]	2.1 [91]	1.96	0.14	1.90	0.20	1.96	0.14	0.12	1.98	1.70	0.4
$KCaF_3$	10.86 [92]	1.388 (583.9 nm) [61]	1.46	0.07	1.33	0.06	1.72	0.33	N.V.	N.D.	1.38	0.01
$LiBaF_3$	9.8 [76]	1.544 (632.8 nm) [73]	1.45	0.09	1.36	0.18	1.76	0.22	N.V.	N.D.	1.43	0.11
$KZnF_3$	7.237 [93]	1.53 (583.9 nm) [61]	1.59	0.06	1.47	0.06	1.90	0.37	N.V.	N.D.	1.62	0.09
$RbCaF_3$	10.9 [94]	1.46 [95]	1.47	0.01	1.33	0.13	1.72	0.26	N.V.	N.D.	1.38	0.08
$CsCaCl_3$	6.89 [96]	1.58, 1.603 (583.9 nm) [61,96]	1.54	0.04, 0.06	1.49	0.09, 0.11	1.93	0.35, 0.33	N.V.	N.D.	1.65	0.07, 0.05

N.V. represents a negative value MAE, 0.07, 0.11, 0.23, 0.87, 0.21. N.D. represents not defined.

II. Consistency of the model: As mentioned above, the experimental values of the direct energy gap and the refractive index values at low frequency are not frequently available for various perovskite materials. Moreover, the searched values were not as unique as they depended on the experimental methods used in the literature. Further, a few papers mentioned the phases and distortion of the structure before measuring the energy gap. Such inconsistency may impede the validity of the model. In order to remove such inconsistency, the energy gap values were taken from one common source [97] obtained from density functional theory (DFT) using the HSE (Heyd–Scuseria–Ernzerhof) functional. The results are shown in Tables 2 and 3. We also included some available values of the refractive index in the last columns of these tables. They can serve as a reference and may be used with caution in comparing with other computed values. This is because of the fact that all the computed values of the refractive indices are a function of their respective energy gaps, and it is well known that the computed energy gaps using HSE underestimate the actual energy gaps [98]. Moreover, their structural phases may not be the same. For instance, in Table 3, the value of the refractive index (as shown by the last column) for orthorhombic (Pnma) $CsNaF_3$ is 4.56, whose energy gap is 0.019 eV as calculated by DFT using the GGA (generalized gradient approximation) functional, whereas the energy gap for cubic (Pm3m) $CsNaF_3$ is 0.26 eV using the HSE functional. Our model predicted a higher value of the refractive index for the energy gap close to zero, which was consistent for conducting materials. These results can be seen in Figures 2 and 3. At higher energy gaps, this model converged with the Wemple–DiDomenico, Moss, and Herve–Vandamme models. One can notice that the prediction of the refractive index by the Ravindra relation showed negative values when the corresponding energy gaps were above 6.6 eV. This could be attributed to the non-parallelism in the trajectories of valence and conduction bands along the symmetry directions in perovskites [99–101]. Overall, the tabulated values indicated that Equations (13a) and (13b) were consistent enough for oxide perovskites and halide perovskites.

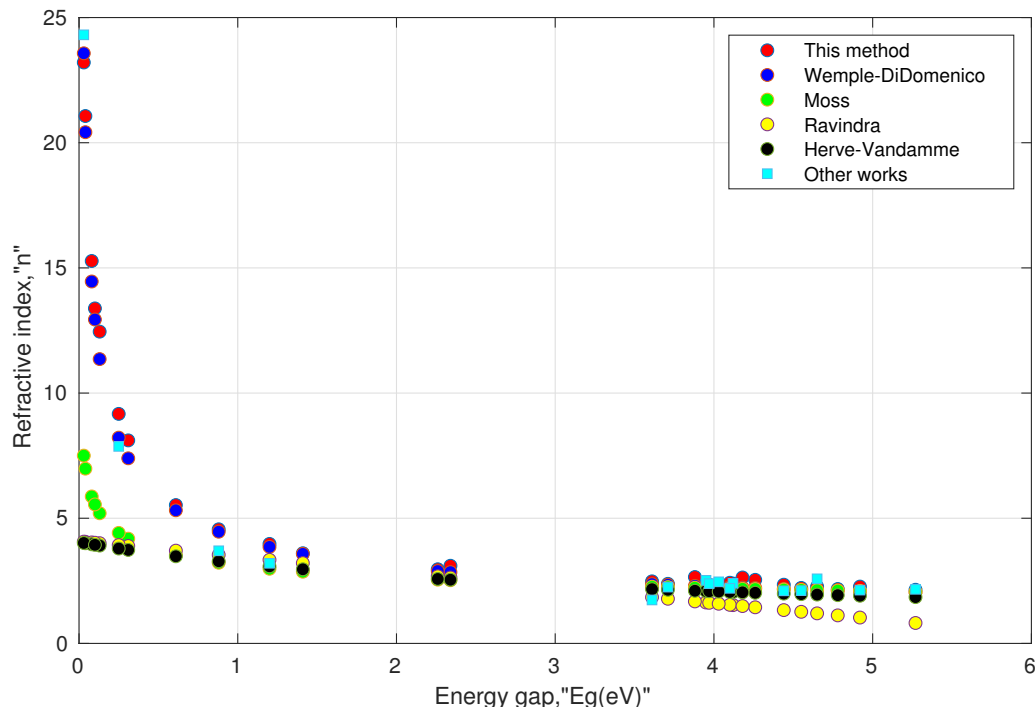


Figure 2. Simulated behavior of various models for oxide perovskites, shown in Table 2.

So far, we have seen that the proposed model not only predicts the refractive index of the perovskites with sufficient accuracy, but also shows a consistent behavioral pattern with some of the well-established models. However, it may not be appropriate to claim that the new formula is superior to these established models. First of all, the Wemple–DiDomenico model, Moss model, Ravindra

model, and Herve–Vandamme model can be applied to all kinds of materials. However, the behavior of these models depends on various factors such as the types of bonds, the energy gaps, the nature of the materials like unary, binary, or ternary, etc. Secondly, all these models take a single argument, i.e., the smallest direct energy gap to compute the corresponding static refractive index. However, the proposed new formula could be applicable only to perovskites, and it takes two arguments: one is a structural parameter, quantified as the cation-anion ratio, and the other is the energy gap. Generally, perovskites are sensitive to an external stimulus, and therefore, the question of the stability of this structure is very crucial as many electro-optical properties depend on the evolution of the lattice. Therefore, one cannot solely depend on Wemple–DiDomenico model, Moss model, Ravindra model, and Herve–Vandamme model for perovskites as these models isolate structural reformation.

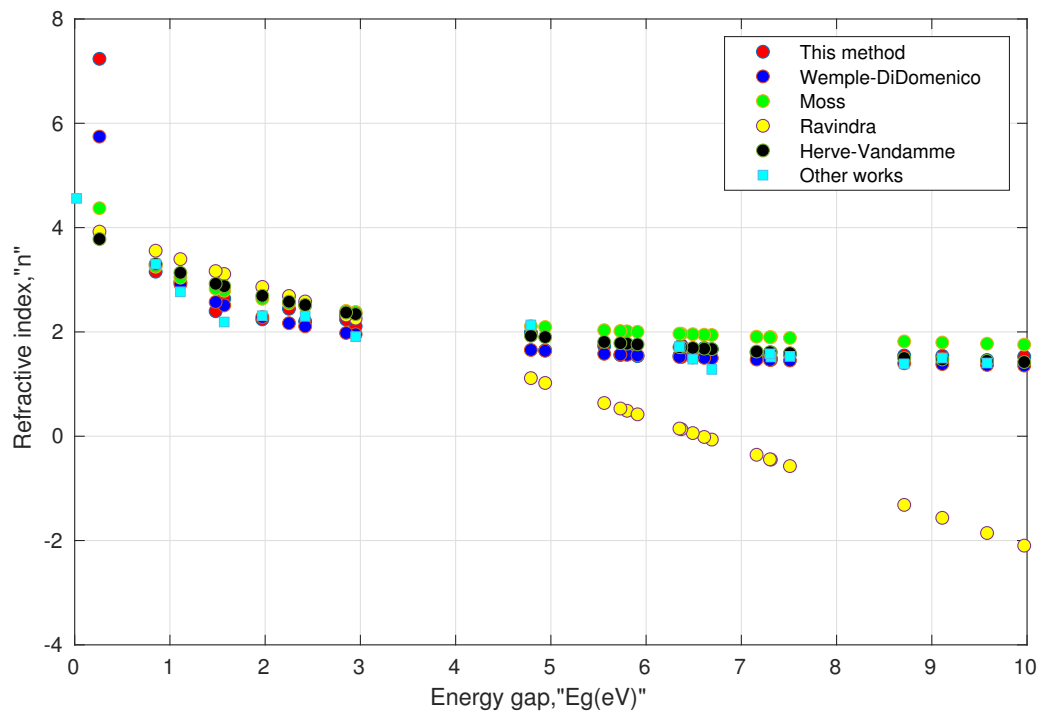


Figure 3. Simulated behavior of various models for halide perovskites, shown in Table 3.

Table 2. Energy gap of various oxide perovskites with their corresponding refractive indices computed from various models.

Oxide Perovskite ABO_3	Energy Gap (HSE) ' E_g (eV)' [97]	$\frac{(n_A + n_B)}{2}$ [102]	This Method (Equation (13a))	Wemple–DiDomenico Relation (Equation (12a))	Moss Relation (Equation (1))	Ravindra Relation (Equation (4))	Herve–Vandamme Relation (Equation (5))	Other Works
<i>PbTiO₃</i>	3.95	0.78	2.38	2.28	2.21	1.64	2.09	≈2.52 [80]
<i>BaNbO₃</i>	0.31	0.85	8.11	7.39	4.18	3.89	3.73	—
<i>BaTiO₃</i>	4.12	0.82	2.39	2.24	2.19	1.53	2.05	≈2.4 [103]
<i>KTaO₃</i>	4.1	0.84	2.42	2.25	2.19	1.54	2.06	≈2.2 (632.8 nm) [73]
<i>NaNbO₃</i>	4.55	0.75	2.22	2.16	2.14	1.26	1.97	≈2.11 [104]
<i>SrFeO₃</i>	1.2	0.75	3.97	3.86	2.98	3.34	3.08	≈3.2 [105]
<i>SrVO₃</i>	0.04	0.75	21.07	20.42	6.98	4.06	4.00	—
<i>KTcO₃</i>	0.13	0.85	12.45	11.36	5.20	4.00	3.91	—
<i>TlIO₃</i>	4.26	0.98	2.54	2.21	2.17	1.44	2.02	—
<i>CsIO₃</i>	4.18	1.05	2.63	2.23	2.18	1.49	2.04	—
<i>CaFeO₃</i>	1.41	0.71	3.60	3.58	2.87	3.21	2.96	—
<i>BaZrO₃</i>	4.92	0.86	2.27	2.09	2.09	1.03	1.90	≈2.13 [89]
<i>BaSnO₃</i>	2.34	0.85	3.10	2.85	2.52	2.63	2.54	—
<i>KNbO₃</i>	4.44	0.84	2.35	2.18	2.15	1.33	1.99	≈2.1 [103]
<i>SrTiO₃</i>	3.97	0.76	2.35	2.28	2.21	1.62	2.08	≈2.388 (632.8 nm) [73]
<i>RbIO₃</i>	3.88	0.99	2.65	2.30	2.22	1.68	2.10	—
<i>BaBiO₃</i>	0.25	0.88	9.17	8.22	4.42	3.93	3.79	7.87 * [106]
<i>SrNbO₃</i>	0.08	0.79	15.28	14.46	5.87	4.03	3.96	—
<i>SrCrO₃</i>	0.61	0.76	5.53	5.32	3.53	3.71	3.48	—
<i>PbZrO₃</i>	4.65	0.82	2.27	2.14	2.13	1.20	1.95	≈2.58 [107]
<i>NaTaO₃</i>	4.78	0.75	2.17	2.12	2.11	1.12	1.93	—
<i>LaNiO₃</i>	0.03	0.68	23.21	23.57	7.50	4.07	4.01	24.31 ** [108]
<i>AgTaO₃</i>	3.61	0.79	2.48	2.37	2.26	1.85	2.17	≈1.736 [109]
<i>SrZrO₃</i>	5.27	0.80	2.14	2.04	2.06	0.82	1.85	≈2.16 [90]
<i>LaCrO₃</i>	3.71	0.73	2.38	2.34	2.25	1.78	2.14	≈ 2.25 [110]
<i>LaMnO₃</i>	2.26	0.74	2.96	2.89	2.55	2.68	2.58	—
<i>CaTiO₃</i>	4.03	0.74	2.32	2.26	2.20	1.59	2.07	≈2.46 [78]
<i>LaTiO₃</i>	0.1	0.75	13.38	12.94	5.55	4.02	3.94	—
<i>SrCoO₃</i>	0.88	0.74	4.56	4.46	3.22	3.54	3.28	≈3.7 [105]

* Estimate based on reflectivity of 0.6 at 0 K; ** estimate based on reflectivity of 0.85 at 0 K.

Table 3. Energy gap of various halide perovskites with their corresponding refractive indices computed from various models.

Halide Perovskite ABX_3	Energy Gap (HSE) E_g (eV) [97]	$\frac{(r_A + r_B)}{2r_X}$ [102]	This Method (Equation (13b))	Wemple–DiDomenico Relation (Equation (12b))	Moss Relation (Equation (1))	Ravindra Relation (Equation (4))	Herve–Vandamme Relation (Equation (5))	Other Works
<i>TlZnF₃</i>	5.8	0.95	1.71	1.56	2.01	0.49	1.78	–
<i>CsSnCl₃</i>	1.57	0.79	2.64	2.51	2.79	3.11	2.88	≈2.19 [111]
<i>CsGeI₃</i>	1.48	0.59	2.40	2.57	2.83	3.17	2.92	–
<i>KMgF₃</i>	9.58	0.92	1.46	1.37	1.77	N.V.	1.44	≈1.404 (632.8 nm) [73]
<i>KCdF₃</i>	6.69	1.01	1.67	1.50	1.94	N.V.	1.67	≈ 1.28 [96]
<i>RbZnF₃</i>	7.16	0.96	1.61	1.47	1.91	N.V.	1.62	–
<i>RbCaF₃</i>	9.11	1.06	1.54	1.38	1.80	N.V.	1.47	≈1.5 [112]
<i>RbCdF₃</i>	6.61	1.04	1.69	1.50	1.95	N.V.	1.68	–
<i>RbCaCl₃</i>	7.31	0.76	1.49	1.46	1.90	N.V.	1.61	≈1.52 [112]
<i>RbMnF₃</i>	6.49	0.99	1.68	1.51	1.96	0.06	1.69	≈1.478 [61]
<i>CsNaF₃</i>	0.26	1.13	7.24	5.74	4.37	3.92	3.78	4.56 * [90,97]
<i>TlCdBr₃</i>	5.91	0.68	1.54	1.55	2.00	0.42	1.76	–
<i>RbNiF₃</i>	5.56	0.94	1.73	1.58	2.03	0.64	1.81	–
<i>CsCaF₃</i>	9.97	1.12	1.53	1.35	1.76	N.V.	1.42	–
<i>CsPbF₃</i>	4.79	1.19	1.99	1.65	2.11	1.11	1.93	≈2.134 (5.7 eV) [81]
<i>CsSnBr₃</i>	1.11	0.72	2.96	2.91	3.04	3.39	3.13	≈2.769 [111]
<i>CsCdF₃</i>	6.37	1.10	1.74	1.52	1.96	0.13	1.70	–
<i>KZnF₃</i>	7.51	0.93	1.57	1.45	1.88	N.V.	1.59	≈1.53 (583.9 nm) [61]
<i>CsCaCl₃</i>	7.3	0.80	1.52	1.46	1.90	N.V.	1.61	≈1.58, 1.603 (583.9 nm) [61,96]
<i>CsGeBr₃</i>	1.97	0.67	2.24	2.28	2.63	2.86	2.69	≈2.31 [113]
<i>CsPbBr₃</i>	2.42	0.79	2.20	2.11	2.50	2.58	2.52	≈ 2.3 (580 nm) [85]
<i>CsCaBr₃</i>	6.35	0.74	1.54	1.52	1.97	0.15	1.71	≈1.72 [90]
<i>CsPbCl₃</i>	2.95	0.86	2.11	1.95	2.38	2.25	2.34	≈1.91 [86]
<i>CsSnI₃</i>	0.85	0.64	3.15	3.28	3.25	3.56	3.30	≈3.3 [111]
<i>KCaF₃</i>	8.71	1.03	1.55	1.40	1.82	N.V.	1.50	≈ 1.388 (583.9 nm) [61]
<i>KMnCl₃</i>	5.73	0.69	1.56	1.56	2.02	0.53	1.78	–
<i>TlFeF₃</i>	2.85	0.96	2.24	1.98	2.40	2.32	2.37	–
<i>LiSnCl₃</i>	4.94	0.72	1.65	1.64	2.09	1.02	1.90	–
<i>TlCuF₃</i>	2.25	0.95	2.44	2.17	2.55	2.69	2.58	–

N.V. represents a negative value; * orthorhombic lattice, $E_g = 0.019$ eV.

5. Conclusions

In summary, this study presented a new model to correlate the refractive index with the energy gap in perovskites. This model was tested on various oxide perovskites and halide perovskites, and the results obtained were in accord with some established models, as well as the literature values. All these models facilitated the calculation of the static refractive index based on the transition of valence electrons to the conduction band after absorbing the threshold photon energy, and henceforth, all these were discrete models. The efficacy of the proposed model was that it represented the correct picture of optical and electronic properties depending on the structural evolution in perovskites. It took account of both structural distortion and the covalent nature of the $B - X$ bond that were responsible for the fluctuations of the optoelectronic properties. Moreover, it is a well-established fact that the optoelectronic properties are susceptible to the structural reorganization in perovskites. Therefore, the more precise the measurement of the cation/anion ratio, the more accurate will be the correlation predicted by this model.

Author Contributions: The authors contributed equally to this work. All authors have read and agreed to the published version of the manuscript.

Funding: No external funds have been received in support of this work.

Acknowledgments: The authors are thankful to MDPI for its support.

Conflicts of Interest: The authors declare that they have no conflict of interest.

References

1. Johnsson, M.; Lemmens, P. Crystallography and Chemistry of Perovskites. In *Handbook of Magnetism and Advanced Magnetic Materials*; John Wiley: Hoboken, NJ, USA, 2007. Available online: <https://onlinelibrary.wiley.com/doi/abs/10.1002/9780470022184.hmm411> (accessed on 11 January 2020).
2. Varma, P.R. Chapter 7—Low-Dimensional Perovskites. In *Perovskite Photovoltaics*; Thomas, S., Thankappan, A., Eds.; Academic Press: Cambridge, MA, USA, 2018; pp. 197–229. Available online: <http://www.sciencedirect.com/science/article/pii/B9780128129159000071> (accessed on 11 January 2020). [CrossRef]
3. Hussain, I.; Tran, H.P.; Jaksik, J.; Moore, J.; Islam, N.; Uddin, M.J. Functional materials, device architecture, and flexibility of perovskite solar cell. *Emerg. Mater.* **2018**, *1*, 133–154. [CrossRef]
4. Young, J.; Rondinelli, J.M. Octahedral Rotation Preferences in Perovskite Iodides and Bromides. *J. Phys. Chem. Lett.* **2016**, *7*, 918–922. [CrossRef]
5. Dogan, F.; Lin, H.; Guilloux-Viry, M.; Peña, O. Focus on properties and applications of perovskites. *Sci. Technol. Adv. Mater.* **2015**, *16*, 020301. [CrossRef]
6. Dai, X.; Xu, K.; Wei, F. Recent progress in perovskite solar cells: The perovskite layer. *Beilstein J. Nanotechnol.* **2020**, *11*, 51–60. [CrossRef]
7. Mao, Y.; Zhou, H.; Wong, S.S. Synthesis, Properties, and Applications of Perovskite - Phase Metal Oxide Nanostructures. *Mater. Matters* **2010**, *5*, 50. Available online: <https://www.sigmaaldrich.com/content/dam/sigma-aldrich/articles/material-matters/pdf/synthesis-properties.pdf> (accessed on 15 January 2020).
8. Petrović, M.; Chellappan, V.; Ramakrishna, S. Perovskites: Solar cells and engineering applications—materials and device developments. *Solar Energy* **2015**, *122*, 678–699. [CrossRef]
9. Schneemeyer, L.; Waszczak, J.; Zahorak, S.; van Dover, R.; Siegrist, T. Superconductivity in rare earth cuprate perovskites. *Mater. Res. Bull.* **1987**, *22*, 1467–1473. [CrossRef]
10. Li, W.; Ji, L.J. Perovskite ferroelectrics go metal free. *Science* **2018**, *361*, 132. [CrossRef] [PubMed]
11. Assirey, E.A.R. Perovskite synthesis, properties and their related biochemical and industrial application. *Saudi Pharm. J.* **2019**, *27*, 817–829. [CrossRef] [PubMed]
12. Wei, H.; Huang, J. Halide lead perovskites for ionizing radiation detection. *Nat. Commun.* **2019**, *10*, 1066. [CrossRef]
13. Liu, X.; Zhao, W.; Cui, H.; Xie, Y.; Wang, Y.; Xu, T.; Huang, F. Organic-inorganic halide perovskite based solar cells—Revolutionary progress in photovoltaics. *Inorg. Chem. Front.* **2015**, *2*. [CrossRef]

14. Jayatissa, A.; Shi, Z. Perovskites-Based Solar Cells: A Review of Recent Progress, Materials and Processing Methods. *Materials* **2018**, *11*, 729.
15. Wells, H. Über die Cäsium- und Kalium-Bleihalogenide. *Zeitschrift für Anorganische Chemie* **2004**, *3*, 195–210. [[CrossRef](#)]
16. Møller, C.K. *The Structure of Caesium Plumbo Iodide CsPbI₃*; Matematisk-Fysiske Meddelelser bd. 32, nr. 1; Danske videnskabernes selskab: Copenhagen, Denmark, 1959.
17. Kojima, A.; Teshima, K.; Shirai, Y.; Miyasaka, T. Organometal Halide Perovskites as Visible-Light Sensitizers for Photovoltaic Cells. *J. Am. Chem. Soc.* **2009**, *131*, 6050–6051. [[CrossRef](#)]
18. Zhang, C.; Manohari, A.G.; Liu, C.; Hu, J.; Yang, Y.; Schropp, R.; Mai, Y. Inorganic halide perovskite materials and solar cells. *APL Mater.* **2019**, *7*, 120702. [[CrossRef](#)]
19. Pasanen, H.P.; Vivo, P.; Canil, L.; Abate, A.; Tkachenko, N. Refractive index change dominates the transient absorption response of metal halide perovskite thin films in the near infrared. *Phys. Chem. Chem. Phys.* **2019**, *21*, 14663–14670. [[CrossRef](#)]
20. Xiao, W.; Tan, D.; Zhou, W.; Liu, J.; Xu, J. Cubic perovskite polymorph of strontium metasilicate at high pressures. *Am. Mineral.* **2013**, *98*, 2096–2104. [[CrossRef](#)]
21. Dalpian, G.; Wang, Z.; Zunger, A. The polymorphous nature of cubic halide perovskites. *arXiv* **2019**, arXiv:1905.09141.
22. Wang, P.; Guan, J.; Galeschuk, D.T.K.; Yao, Y.; He, C.F.; Jiang, S.; Zhang, S.; Liu, Y.; Jin, M.; Jin, C.; et al. Pressure-Induced Polymorphic, Optical, and Electronic Transitions of Formamidinium Lead Iodide Perovskite. *J. Phys. Chem. Lett.* **2017**, *8*, 2119–2125. [[CrossRef](#)]
23. Ou, Q.; Bao, X.; Zhang, Y.; Shao, H.; Xing, G.; Li, X.; Shao, L.; Bao, Q. Band structure engineering in metal halide perovskite nanostructures for optoelectronic applications. *Nano Mater. Sci.* **2019**, *1*, 268–287. [[CrossRef](#)]
24. Hu, Z.; Lin, Z.; Su, J.; Zhang, J.; Chang, J.; Hao, Y. A Review on Energy Band-Gap Engineering for Perovskite Photovoltaics. *Solar RRL* **2019**. [[CrossRef](#)]
25. Geng, T.; Ma, Z.; Chen, Y.; Cao, Y.; Lv, P.; Li, N.; Xiao, G. Bandgap engineering in two-dimensional halide perovskite Cs₃Sb₂I₉ nanocrystals under pressure. *Nanoscale* **2020**, *12*, 1425–1431. [[CrossRef](#)] [[PubMed](#)]
26. Wu, M.J.; Kuo, C.C.; Jhuang, L.S.; Chen, P.H.; Lai, Y.F.; Chen, F.C. Bandgap Engineering Enhances the Performance of Mixed-Cation Perovskite Materials for Indoor Photovoltaic Applications. *Adv. Energy Mater.* **2019**, *9*, 1901863. [[CrossRef](#)]
27. Ravindra, N.; Ganapathy, P.; Choi, J. Energy gap–refractive index relations in semiconductors—An overview. *Infrared Phys. Technol.* **2007**, *50*, 21–29. [[CrossRef](#)]
28. Tripathy, S.K.; Pattanaik, A. Optical and electronic properties of some semiconductors from energy gaps. *Opt. Mater.* **2016**, *53*, 123–133. [[CrossRef](#)]
29. Kumar, V.; Singh, J. Model for calculating the refractive index of different materials. *Indian J. Pure Appl. Phys.* **2010**, *48*. Available online: <https://pdfs.semanticscholar.org/23c1/aaa68db93cc2028b96e7144442e3eb26ca41.pdf> (accessed on 13 January 2020)
30. Celliers, P.M.; Millot, M.; Brygoo, S.; McWilliams, R.S.; Fratanduono, D.E.; Rygg, J.R.; Goncharov, A.F.; Loubeyre, P.; Eggert, J.H.; Peterson, J.L.; et al. Insulator-metal transition in dense fluid deuterium. *Science* **2018**, *361*, 677–682. [[CrossRef](#)]
31. Kushnir, O.; Shchepanskyi, P.; Stadnyk, V.; Fedorchuk, A. Relationships among optical and structural characteristics of ABSO₄ crystals. *Opt. Mater.* **2019**, *95*, 109221. [[CrossRef](#)]
32. Aziz, S.B.; Hassan, A.Q.; Mohammed, S.J.; Karim, W.O.; Kadir, M.F.Z.; Tajuddin, H.A.; Chan, N.N.M.Y. Structural and Optical Characteristics of PVA:C-Dot Composites: Tuning the Absorption of Ultra Violet (UV) Region. *Nanomaterials* **2019**, *9*, 216. [[CrossRef](#)]
33. Drissi, N.; Bouarissa, N.; Jomni, F. Optical properties and chemical bonding of 3C-SiC under high-pressure. *Optik* **2020**, *202*, 163613. [[CrossRef](#)]
34. Mrdjenovich, D.; Horton, M.K.; Montoya, J.H.; Legaspi, C.M.; Dwaraknath, S.; Tshitoyan, V.; Jain, A.; Persson, K.A. propnet: A Knowledge Graph for Materials Science. *Matter* **2020**, *2*, 464–480. [[CrossRef](#)]
35. Sharma, E.; Sharma, P. Applicability of different models of energy bandgap and refractive index for chalcogenide thin films. *Mater. Today Proc.* **2020**. [[CrossRef](#)]

36. Hoat, D.; Naseri, M.; Ponce-Pérez, R.; Rivas-Silva, J.; Coccoletzi, G.H. First principles insight into the structural, electronic, optical and thermodynamic properties of $CsPb_2Br_5$ compound. *Chem. Phys.* **2020**, *533*, 110704. [CrossRef]
37. Isik, M.; Delice, S.; Gasanly, N.; Darvishov, N.; Bagiev, V. Investigation of optical properties of $Bi_{12}GeO_{20}$ sillenite crystals by spectroscopic ellipsometry and Raman spectroscopy. *Ceram. Int.* **2020**. [CrossRef]
38. Ueda, K.; Yanagi, H.; Noshiro, R.; Hosono, H.; Kawazoe, H. Vacuum ultraviolet reflectance and electron energy loss spectra of $CaTiO_3$. *J. Phys. Condens. Matter* **1998**, *10*, 3669–3677. [CrossRef]
39. Manzoor, S.; Häusele, J.; Bush, K.A.; Palmstrom, A.F.; Carpenter, J.; Yu, Z.J.; Bent, S.F.; McGehee, M.D.; Holman, Z.C. Optical modeling of wide-bandgap perovskite and perovskite/silicon tandem solar cells using complex refractive indices for arbitrary-bandgap perovskite absorbers. *Opt. Express* **2018**, *26*, 27441–27460. [CrossRef]
40. Phillips, L.; Rashed, A.; Treharne, R.; Kay, J.; Yates, P.; Mitrovic, I.; Weerakkody, A.; Hall, S.; Durose, K. Maximizing the optical performance of planar $CH_3NH_3PbI_3$ hybrid perovskite heterojunction stacks. *Solar Energy Mater. Solar Cells* **2015**, *147*, 327–333. [CrossRef]
41. Nyayban, A.; Panda, S.; Chowdhury, A.; Sharma, B.I. First principle studies on the optoelectronic properties of rubidium lead halides. *arXiv* **2019**, arXiv:1909.11419
42. Ezealigo, B.; Nwanya, A.; Ezugwu, S.; Offiah, S.; Obi, D.; Osuji, R.; Bucher, R.; Maaza, M.; Ejikeme, P.; Ezema, F. Method to Control the Optical properties: Band Gap Energy of Mixed Halide Organolead Perovskites. *Arab. J. Chem.* **2017**, *13*. [CrossRef]
43. Nenkov, M.; Pencheva, T. Determination of thin film refractive index and thickness by means of film phase thickness. *Open Phys.* **2008**, *6*, 332–343. [CrossRef]
44. Ono, M.; Aoyama, S.; Fujinami, M.; Ito, S. Significant suppression of Rayleigh scattering loss in silica glass formed by the compression of its melted phase. *Opt. Express* **2018**, *26*, 7942. [PubMed]
45. Ong, H.; Dai, J.; Li, A.; Du, G.; Chang, R.; Ho, S. Effect of a microstructure on the formation of self-assembled laser cavities in polycrystalline ZnO. *J. Appl. Phys.* **2001**, *90*, 1663–1665. [CrossRef]
46. Moss, T.S. Photoconductivity in the Elements. *Proc. Phys. Soc. Sect. A* **1951**, *64*, 590–591. [CrossRef]
47. Moss, T.S. Relations between the Refractive Index and Energy Gap of Semiconductors. *Phys. Status Solidi (b)* **1985**, *131*, 415–427. [CrossRef]
48. Reddy, R.; Ahammed, Y.N. A study on the Moss relation. *Infrared Phys. Technol.* **1995**, *36*, 825–830. [CrossRef]
49. Penn, D.R. Wave-Number-Dependent Dielectric Function of Semiconductors. *Phys. Rev.* **1962**, *128*, 2093–2097. [CrossRef]
50. Ravindra, N.; Auluck, S.; Srivastava, V. On the Penn Gap in Semiconductors. *Phys. Status Solidi (b)* **1979**, *93*, K155–K160. [CrossRef]
51. Gupta, V.P.; Ravindra, N.M. Comments on the Moss Formula. *Phys. Status Solidi (b)* **1980**, *100*, 715–719. [CrossRef]
52. Ravindra, N. Energy gap-refractive index relation—some observations. *Infrared Phys.* **1981**, *21*, 283–285. [CrossRef]
53. Tripathy, S. Refractive Indices of Semiconductors from Energy gaps. *Opt. Mater.* **2015**, *46*, 240–246. [CrossRef]
54. Anani, M.; Mathieu, C.; Hamza, A.; Lebid, S.; Zouaoui, C.; Amar, Y. Model for Calculating the Refractive Index of a III-V Semiconductor. *Comput. Mater. Sci.* **2008**, *41*, 570–575. [CrossRef]
55. Herve, P.; Vandamme, L. General relation between refractive index and energy gap in semiconductors. *Infrared Phys. Technol.* **1994**, *35*, 609–615. [CrossRef]
56. Bahadur, A.; Mishra, M. Correlation Between Refractive Index and Electronegativity Difference for ANB8-N Type Binary Semiconductors. *Acta Phys. Pol. A* **2013**, *123*, 737–740. [CrossRef]
57. Wemple, S.H.; DiDomenico, M. Behavior of the Electronic Dielectric Constant in Covalent and Ionic Materials. *Phys. Rev. B* **1971**, *3*, 1338–1351. [CrossRef]
58. Cushman, C.; Smith, N.; Kaykhaii, M.; Podraza, N.; Linford, M. An Introduction to Modeling in Spectroscopic Ellipsometry, Focusing on Models for Transparent Materials: The Cauchy and Sellmeier Models. *Vacuum Technology & Coating*, June 2016.
59. Brückner, V. *To the Use of Sellmeier Formula*; HfT Leipzig: Bonn, Germany, 2014.
60. Wooten, F. *Optical Properties of Solids*; Academic Press: Cambridge, MA, USA, 1972. Available online: https://books.google.com/books?id=A_dHNRXFq28C (accessed on 7 January 2020).

61. Batsanov, S.; Ruchkin, E.; Poroshina, I. *Refractive Indices of Solids*; Springer Science + Business Media Singapore Pte Ltd.: Singapore, 2016.
62. Koughia, C.; Kasap, S.; Capper, P. *Springer Handbook of Electronic and Photonic Materials*; Springer: Berlin/Heidelberg, Germany, 2007.
63. Efimov, A. *Optical Constants of Inorganic Glasses*; Laser & Optical Science & Technology; Taylor & Francis: Abingdon, UK, 1995. Available online: <https://books.google.com/books?id=A0qMBgqQstwC> (accessed on 23 December 2019).
64. Thankappan, A.; Thomas, S. *Perovskite Photovoltaics: Basic to Advanced Concepts and Implementation*; Academic Press, Elsevier: London, UK, 2019.
65. Walsh, A. Principles of Chemical Bonding and Band Gap Engineering in Hybrid Organic-Inorganic Halide Perovskites. *J. Phys. Chem. C* **2015**, *119*, 5755–5760. [[CrossRef](#)]
66. The ABX_3 Perovskite Structure. In *Perovskites*; John Wiley and Sons, Ltd.: Hoboken, NJ, USA, 2016; Chapter 1, pp. 1–41, [[CrossRef](#)]
67. Lee, J.H.; Bristowe, N.C.; Lee, J.H.; Lee, S.H.; Bristowe, P.D.; Cheetham, A.K.; Jang, H.M. Resolving the Physical Origin of Octahedral Tilting in Halide Perovskites. *Chem. Mater.* **2016**, *28*, 4259–4266, [[CrossRef](#)]
68. Tilley, R. *Perovskites: Structure-Property Relationships*; John Wiley & Sons, Ltd.: Sussex, UK, 2016; pp. 1–315. [[CrossRef](#)]
69. George, J.; Waroquiers, D.; Stefano, D.D.; Petretto, G.; Rignanese, G.M.; Hautier, G. The Limited Predictive Power of the Pauling Rules. 2019. Available online: https://chemrxiv.org/articles/The_Limited_Predictive_Power_of_the_Pauling_Rules/9255446 (accessed on 18 January 2020). [[CrossRef](#)]
70. Moreira, R.L.; Dias, A. Comment on “Prediction of lattice constant in cubic perovskites”. *J. Phys. Chem. Solids* **2007**, *68*, 1617–1622. [[CrossRef](#)]
71. Granger, P.; Parvulescu, V.; Kaliaguine, S.; Prellier, W. *Perovskites and Related Mixed Oxides: Concepts and Applications*; Wiley-VCM: Weinheim, Germany, 2015; pp. 1–978. [[CrossRef](#)]
72. Cammarata, A.; Rondinelli, J.M. Covalent dependence of octahedral rotations in orthorhombic perovskite oxides. *J. Chem. Phys.* **2014**, *141*, 114704. [[CrossRef](#)]
73. Weber, M.J. *Handbook of Optical Materials*; CRC Press: Boca Raton, FL, USA, 2003.
74. Zhang, Y.; Sahoo, M.; Wang, J. Tuning the band gap and polarization in $BaSnO_3/SrSnO_3$ superlattices for photovoltaic applications. *Phys. Chem. Chem. Phys.* **2017**, *19*. [[CrossRef](#)]
75. Schumann, T.; Raghavan, S.; Ahadi, K.; Kim, H.; Stemmer, S. Structure and optical band gaps of $(Ba, Sr)SnO_3$ films grown by molecular beam epitaxy. *J. Vac. Sc. Technol. A Vac. Surf. Films* **2016**, *34*, 050601. [[CrossRef](#)]
76. Ono, S.; Riadh, O.; Quema, A.; Murakami, H.; Sarukura, N.; Nishimatsu, T.; Terakubo, N.; Mizuseki, H.; Kawazoe, Y.; Yoshikawa, A.; et al. Band-Structure Design of Fluoride Complex Materials for Deep-Ultraviolet Light-Emitting Diodes. *Jpn. J. Appl. Phys.* **2005**, *44*, 7285–7290. [[CrossRef](#)]
77. Pradhan, S.A.; Jameson, M.; Sujoy, S.; Sadhan, C.; Alo, D.; Indrajit, S.B.; Thapa, R.K.; Sinha, T.P. Electronic structure and elastic properties of $ATiO_3$ ($A = Ba, Sr, Ca$) perovskites: A first principles study. *IJPAP* **2015**, *53*, 102–109.
78. Rizwan, M.; Usman, Z.; Shakil, M.; Gillani, S.S.A.; Azeem, S.; Jin, H.B.; Cao, C.B.; Mehmood, R.F.; Nabi, G.; Asghar, M.A. Electronic and optical behavior of lanthanum doped $CaTiO_3$ perovskite. *Mater. Res. Express* **2020**, *7*, 015920. [[CrossRef](#)]
79. Piskunov, S.; Heifets, E.; Eglitis, I.; Borstel, G. Bulk properties and electronic structure of $SrTiO_3$, $BaTiO_3$, $PbTiO_3$ perovskites: an ab initio HF/DFT study. *Comput. Mater. Sci.* **2004**, *29*, 165–178. [[CrossRef](#)]
80. Tropf, W.J.; Thomas, M.E.; Harris, T.J. Chapter 33- Properties of Crystals & Glasses. In *Handbook of Optics*; The McGraw-Hill Companies, Inc.: New York, NY, USA, 1995; Available online: http://www.photonics.intec.ugent.be/education/IVPV/res_handbook/v2ch33.pdf (accessed on: 23 November 2019)
81. Murtaza, G.; Ahmad, I.; Maqbool, M.; Aliabad, H.A.R.; Afaq, A. Structural and Optoelectronic Properties of Cubic $CsPbF_3$ for Novel Applications. *Chin. Phys. Lett.* **2011**, *28*, 117803. [[CrossRef](#)]
82. Singh, R.K.; Kumar, R.; Jain, N.; Dash, S.R.; Singh, J.; Srivastava, A. Investigation of optical and dielectric properties of $CsPbI_3$ inorganic lead iodide perovskite thin film. *J. Taiwan Inst. Chem. Eng.* **2019**, *96*, 538–542. [[CrossRef](#)]
83. Jellison, G.E.; Paulauskas, I.; Boatner, L.A.; Singh, D.J. Optical functions of $KTaO_3$ as determined by spectroscopic ellipsometry and comparison with band structure calculations. *Phys. Rev. B* **2006**, *74*, 155130. [[CrossRef](#)]

84. Yuan, Y.; Xu, R.; Xu, H.T.; Hong, F.; Xu, F.; Wang, L. Nature of the band gap of halide perovskites ABX_3 ($A = CH_3NH_3, Cs$; $B = Sn, Pb$; $X = Cl, Br, I$): First-principles calculations. *Chin. Phys. B* **2015**, *24*, 116302. [[CrossRef](#)]
85. Dirin, D.; Cherniukh, I.; Yakunin, S.; Shynkarenko, Y.; Kovalenko, M. Solution-Grown $CsPbBr_3$ Perovskite Single Crystals for Photon Detection. *Chem. Mater.* **2016**, *28*. [[CrossRef](#)]
86. Database, M. Available online: <http://webmineral.com/data/Perovskite.shtml.XraySG5NKjOR> (accessed on 13 December 2019).
87. Estrada, R.; Djohan, N.; Pasole, D.; Dahrul, M.; Kurniawan, A.; Iskandar, J.; Hardhienata, H.; Irzaman. The optical band gap of $LiTaO_3$ and Nb_2O_5 -doped $LiTaO_3$ thin films based on Tauc Plot method to be applied on satellite. *IOP Conf. Ser. Earth Environ. Sci.* **2017**, *54*, 012092. [[CrossRef](#)]
88. Pilia, G.; McClellan, K.; Stanek, C.; Uberuaga, B. Physics-informed machine learning for inorganic scintillator discovery. *J. Chem. Phys.* **2018**, *148*. [[CrossRef](#)] [[PubMed](#)]
89. Kouchaksaraie, L.S. Theoretical Calculation of Electrical and Optical Properties of $BaZrO_3$. *Int. J. Phys. Math. Sci.* **2011**, *5*, 1680–1683.
90. Jain, A.; Ong, S.P.; Hautier, G.; Chen, W.; Richards, W.D.; Dacek, S.; Cholia, S.; Gunter, D.; Skinner, D.; Ceder, G.; et al. The Materials Project: A materials genome approach to accelerating materials innovation. *APL Mater.* **2013**, *1*, 011002. [[CrossRef](#)]
91. Database, M. Available online: <http://www.webmineral.com/data/Lakargiite.shtml#XbRoEugzbIU> (accessed on 17 November 2019).
92. Babu, K.E.; Murali, N.; Babu, K.; Babu, B.; Veeraiyah, V. Structural, electronic and elastic properties of $KCaF_3$ and $RbCaF_3$ for vacuumultraviolet- transparent lens materials. *AIP Conf. Proc.* **2015**, *1661*, 100002. [[CrossRef](#)]
93. Hiadsi, S.; Bouafia, H.; Sahli, B.; Abidri, B.; Bouaza, A.; Akriche, A. Structural, mechanical, electronic and thermal properties of $KZnF_3$ and $AgZnF_3$ Perovskites: FP-(L)APW+lo calculations. *Solid State Sci.* **2016**, *58*, 1–13. [[CrossRef](#)]
94. Ehsan, S.; Tröster, A.; Tran, F.; Blaha, P. DFT study of the electronic properties and the cubic to tetragonal phase transition in $RbCaF_3$. *Phys. Rev. Mater.* **2018**, *2*. [[CrossRef](#)]
95. Mousa, A.; Khalifeh, J.; Mahmoud, N.; Juwhari, H. First Principles Study of Structural, Electronic and Optical Properties of the Fluoroperovskite $RbCaF_3$ Crystal. *Am. J. Condens. Matter Phys.* **2013**, *3*, 151–162. [[CrossRef](#)]
96. Lal, M.; Kapila, S. Structural, electronic, optical and mechanical properties of $CsCaCl_3$ and $KCdF_3$ cubic perovskites. *Int. J. Mater. Sci.* **2017**, *12*, 137–147.
97. Körbel, S.; Marques, M.A.L.; Botti, S. Stability and electronic properties of new inorganic perovskites from high-throughput ab initio calculations. *J. Mater. Chem. C* **2016**, *4*, 3157–3167. [[CrossRef](#)]
98. Garza, A.; Scuseria, G. Predicting Band Gaps with Hybrid Density Functionals. *J. Phys. Chem. Lett.* **2016**, *7*. [[CrossRef](#)] [[PubMed](#)]
99. Takegahara, K. Electronic band structures in cubic perovskite-type oxides: Bismuthates and transition metal oxides. *J. Electron Spectrosc. Relat. Phenom.* **1994**, *66*, 303–320. [[CrossRef](#)]
100. Whalley, L.D.; Frost, J.M.; Jung, Y.K.; Walsh, A. Perspective: Theory and simulation of hybrid halide perovskites. *J. Chem. Phys.* **2017**, *146*, 220901, [[CrossRef](#)] [[PubMed](#)]
101. Green, M.A.; Jiang, Y.; Soufiani, A.M.; Ho-Baillie, A. Optical Properties of Photovoltaic Organic–Inorganic Lead Halide Perovskites. *J. Phys. Chem. Lett.* **2015**, *6*, 4774–4785. [[CrossRef](#)] [[PubMed](#)]
102. Jiang, L.; Guo, J.; Liu, H.; Zhu, M.; Zhou, X.; Wu, P.; Li, C. Prediction of lattice constant in cubic perovskites. *J. Phys. Chem. Solids* **2006**, *67*, 1531–1536. [[CrossRef](#)]
103. Polyanskiy, M.N. Refractive Index Database. Available online: <https://refractiveindex.info> (accessed on 13 March 2020).
104. Lingwal, V.; Kandari, A.S.; Panwar, N.S. Optical properties of sodium niobate thin films. *Nanosyst. Phys. Chem. Math.* **2016**, 583–591. [[CrossRef](#)]
105. Jia, T.; Zeng, Z.; Lin, H.Q.; Duan, Y.; Ohodnicki, P. First-principles study on the electronic, optical and thermodynamic properties of ABO_3 ($A = La, Sr$, $B = Fe, Co$) perovskites. *RSC Adv.* **2017**, *7*, 38798–38804. [[CrossRef](#)]
106. Lobo, R.P.S.M.; Gervais, F.M.C. Bismuth disproportionation in $BaBiO_3$ studied by infrared and visible reflectance spectra. *Phys. Rev. B* **1995**, *52*, 13294–13299. [[CrossRef](#)]

107. Nazir, G.; Tariq, S.; Afaq, A.; Mahmood, Q.; Saad, S.; Mahmood, A.; Tariq, S. Under Pressure DFT Investigations on Optical and Electronic Properties of $PbZrO_3$. *Acta Phys. Pol. A* **2018**, *133*, 105–113. [[CrossRef](#)]
108. Guan, L.; Liu, B.; Jin, L.; Guo, J.; Zhao, Q.; Wang, Y.; Fu, G. Electronic structure and optical properties of $LaNiO_3$: First-principles calculations. *Solid State Commun.* **2010**, *150*, 2011–2014. [[CrossRef](#)]
109. Çabuk, S.; Simsek, S. First-principles studies of the electronic structure and optical properties of $AgBO_3$ (B = Nb, Ta) in the paraelectric phase. *Open Phys.* **2008**, *6*, 730–736. [[CrossRef](#)]
110. Soltani, N.; Hosseini, S.; Kompany, A. Nanoscale ab-initio calculations of optical and electronic properties of $LaCrO_3$ in cubic and rhombohedral phases. *Phys. B-Condens. Matter* **2009**, *404*, 4007–4014. [[CrossRef](#)]
111. Ayatullah, K.; Murtaza, G.; Muhammad, S.; Naeem, S.; Khalid, M.; Ali, M. Physical properties of $CsSnM_3$ (M = Cl, Br, I): A first principle study. *Acta Phys. Pol. A* **2013**, *124*, 102–107. [[CrossRef](#)]
112. Mubarak, A. The elastic, electronic and optical properties of $RbCaX_3$ (X = F, Cl) compounds. *Int. J. Mod. Phys. B* **2014**, *28*, 1450192. [[CrossRef](#)]
113. Tang, L.C.; Huang, J.; Chang, C.; Lee, M.H.; Liu, L. New infrared nonlinear optical crystal $CsGeBr_3$: Synthesis, structure and powder second-harmonic generation properties. *J. Phys. Condens. Matter* **2005**, *17*, 217–275. [[CrossRef](#)]



© 2020 by the authors. Licensee MDPI, Basel, Switzerland. This article is an open access article distributed under the terms and conditions of the Creative Commons Attribution (CC BY) license (<http://creativecommons.org/licenses/by/4.0/>).